Submitted to ApJ

High-Resolution N-Band Observations of the Nova RS Ophiuchi with the Keck Interferometer Nuller

R. K. Barry[1,2], W. C. Danchi[1], J. L. Sokoloski[3], C. Koresko[4], J. P. Wisniewski[1], E. Serabyn[4], W. Traub[4], M. Kuchner[1], , M. A. Greenhouse[1]

Richard.K.Barry@nasa.gov

ABSTRACT

We report new observations of the nova RS Ophiuchi (RS Oph) using the Keck Interferometer Nulling Instrument, approximately 3.8 days following the most recent outburst that occurred on 2006 February 12. The Keck Interferometer Nuller (KIN) operates in N-band from 8 to 12.5 μm in a nulling mode, which means that the central broad-band interference fringe is a dark fringe - with an angular width of 25 mas at mid band - rather than the bright fringe used in a conventional optical interferometer. In this mode the stellar light itself is suppressed by the destructive fringe, effectively enhancing the contrast of the circumstellar material located near the star. By subsequently shifting the neighboring bright fringe onto the center of the source brightness distribution and integrating, a second spatial regime dominated by light from the central portion of the source is almost simultaneously sampled. The nulling technique is the sparse aperture equivalent of the conventional corongraphic technique used in filled aperture telescopes. By fitting the unique KIN inner and outer spatial regime data, we have obtained an angular size of the mid-infrared continuum of 6.2, 4.0, or 5.4 mas for a disk profile, gaussian profile (fwhm), and shell profile respectively. The data show evidence of enhanced neutral atomic hydrogen emission located in the inner spatial regime relative to the outer regime. There is also evidence of a 9.7 micron silicate feature seen outside of this region. Importantly, we see spectral lines excited by the nova flash in the outer region before the blast wave reaches these regions. These lines are from neutral, weakly excited atoms which support

[1]NASA Goddard Space Flight Center, Exoplanets and Stellar Astrophysics Laboratory, Greenbelt, MD 20771

[2]Department of Physics and Astronomy, The Johns Hopkins University, Baltimore, MD 21218

[3]Columbia University, Department of Physics, New York, NY

[4]California Institute of Technology, Jet Propulsion Laboratory, Pasadena, CA

the following interpretation. We discuss the present results in terms of a unifying model of the system that includes an increase in density in the plane of the orbit of the two stars created by a spiral shock wave caused by the motion of the stars through the cool wind of the red giant star. These data show the power and potential of the nulling technique which has been developed for the detection of Earth-like planets around nearby stars for the Terrestrial Planet Finder Mission and Darwin missions.

Subject headings: novae: cataclysmic variables — stars: dwarf novae — stars: individual(RS Ophiuchi, HD162214)— techniques: interferometric— techniques:high angular resolution

1. Introduction

Novae produce many of the elements heavier than helium in the Universe by the entrainment of metal-enriched surface layers of the white dwarf (WD)component of these binary stellar systems during unbound TNR outer-shell fusion reactions. In some cases, typified by the nova T CrB, the WD shares a long-period orbit with a red giant (RG) companion and is embedded in its wind nebula. The ejecta of the surface TNR event expand freely for a period of time then plow into the nebula, producing a characteristic X-ray signature and a rapid narrowing of emission lines as the explosion products decelerate. An important subclass of novae are the repeating novae (RN) which are thought to be progenitors of Type Ia supernovae because their WD component is close to the Chandrasekhar mass limit. We are fortunate to have the RN, T Crb class nova RS Ophiuchi (RS Oph) as a nearby laboratory to advance our understanding of these important objects. The nova RS Ophiuchi (RS Oph) has undergone six recorded episodic outbursts of irregular interval in 1898 (Fleming 1904), 1933 (Adams & Joy 1933), 1958 (Wallerstein 1958), 1967 (Barbon, Mammano & Rosino 1969), 1985 (Morrison 1985) and now 2006. There are also two possible outbursts in 1907 (Schaeffer 2004) and 1945 (Oppenheimer & Mattei 1993). Both of these events occurred during solar inferior conjunction with the 1907 outburst inferred from a post-eruption dip on photographs in the Harvard Collection. The 1945 outburst was inferred from a Fourier analysis conducted on all historic V-band AAVSO photometry of the object leading to the detection of a surge in the objects brightness on JD 2431784 thought to be a nascent outburst. Further scrutiny of the historical V-band data, after the seasonal observing gap for the northern hemisphere, showed a distinct dip in the object's brightness similar in character to that of other events post-outburst.

All outbursts have shown very similar light curves. This system is a single-line binary,

cataclysmic variable with red giant secondary characterized as K5.7 ± 0.4 I-II (Kenyon & Fernandez-Castro 1987) to a K7 III (Mürset & Schmid 1999) in quiescence and a white dwarf primary in a 455.72 ± 0.83 day orbit about their common center of mass as measured using single-line radial velocity techniques (Fekel et al. 2000). The circularity of the orbit as adopted by both Fekel and Dobrzycka & Kenyon (1994) is expected, as tidal interaction on the secondary will cause its rotation to tend towards synchronization with the orbital revolution. This will also eventually eliminate initial orbital eccentricity. Oppenheimer and Mattei also looked at all outbursts and found that RS Oph averaged 0.09 magnitudes/day for the first 43 days after outburst. A 2-magnitude drop would then require on average 22 days, establishing RS Oph as a fast nova based on the classification system of Payne-Gaposchkin (1957). It is important to note that in the literature RS Oph is often sited as a M0 - M3 spectral class with luminosity class III (Kenyon & Gallagher 1983; Blair et al., 1983) but these early measurements are much less thorough than Kenyon & Fernandez-Castro (1987) and Mürset & Schmid (1999) that specifically address classification through measurement of molecular indices.

The most recent outburst of the nova RS Oph was discovered at an estimated V-band magnitude of 4.5 by H. Narumi of Ehime, Japan on 2006 February 12.829 UT (Narumi 2006). This is 0.4 magnitudes brighter than its historical average AAVSO V-band magnitude so it is reasonable to take Feb 12.829 (JD 2453779.329) as day zero. The speed of this outburst is characterized by its T_2 and T_3 times which are 4.75 and 10.19 days, respectively. As the WD approaches the 1.44 $M_\odot$ Chandrasekhar limit the amount of mass initially ejected by the thermonuclear runaway (TNR) decreases. It would not, therefore be unreasonable to expect the initial V-band speed of the nova to gradually increase. Indeed it must be the case that the mass of the WD has grown over time. If earlier in its secular evolution it was a 1.0 $M_\odot$ WD and still had a 20 year recurrence time, its accretion rate would have had to be unacceptably high.

There has been a good deal of disagreement about the distance to the RS Oph system in the literature with a surprisingly broad range derived - over a factor of 20 - from 0.57 to as distant as 5.8 kpc (Pottasch 1967) and even 12.3 kpc (Payne-Gaposchkin 1977). As late as 2001, Hachisu & Kato (2001) quite thoroughly and persuasively argued for the nearer distance while early analysis of X-ray data from the Rossi X-ray Timing Explorer seemed to indicate a distance of 2.3 kpc - later revised to 1.6 kpc prior to publication (Sokoloski et al. 2006). This distance determination is of singular importance to the interferometry community as it profoundly effects interpretation of astrometric data (cf. Monnier et al. (2006)). Derivations of distance using envelope expansion parallax from the nova's last epoch (Hjellming et al. (1986) & Snijders, M.A.J. (1985)) and, using new radio observations from the current epoch (Rupin et al., (2006); O'Brien et al., (2006)) establish a distance at

the mid range. The T_3 and T_2 times noted above do constrain the distance to RS Oph and this is worth noting here. If we restrict ourselves to the use of the T_3 time as a more settled figure, and apply the Maximum Magnitude Rate of Decline (MMRD) expression

$$M_{V_{T_3}} = (-11.99 \pm 0.56) + (2.54 \pm 0.35) * \log(T_3) \quad (1)$$

attributed to Downes & Duerbeck (2000) we obtain a range of peak absolute magnitudes for this outburst of $M_{V_{T3}} = -9.43 \pm 0.91$. We de-redden our peak V-band observed magnitude $M_v = 4.5$ (Narumi 2006) using the reddening coefficient $E(B-V) = 0.73 \pm 0.1$ (Snijders, M.A.J. 1985) and and apply $R_v = 3.1$ for Galactic sources (Cardelli, Clayton & Mathis 1989) to obtain, through the expression $A_v = R_v * E(B-V)$, a range of extinctions $A_v = 2.263 \pm 0.31$. Applying the distance modulus equation yields a range of distances of $D_{RSOph} = 2.51 \pm 1.28$ kpc. To this broad range we apply an additional constraint. As first noted by Cassatella et al. (1985), the distance to RS Ophiuchi cannot exceed approximately 2.0 kpc because it's spectrum does not contain evidence of absorption by material in the Carina arm of the Galaxy. Presence of this feature, as evidenced by the relative $+15 \rightarrow +20$ km/s velocity of the Carina arm, is completely lacking in spectra obtained by Cassatella et al. (1985). This finding was convincingly confirmed by the findings of Hjellming et al. (1986) in which the velocity range $+15 \rightarrow +20$ km/s was sought for two objects along the same sight-line. In this work, Hjellming et al. (1986) did not detect the Galactic signature for RS Oph while they did detect it for the neighboring object. We note that this upper constraint is somewhat soft as it is unknown how deep in the Carina arm the object would have to be imbedded to begin to show a measurable 20 km/sec feature. This would bear further analysis through modeling of the density profile of the Galactic arm. Inclusion of the Galactic upper constraint and the MMRD lower constraint calculated above yields a range of distances to the nova RS Ophiuchi of 1.61 ± 0.39 kpc. Although the subject of distance is worthy of more careful examination, given the strength of this evidence we adopt the system distance of 1.6 kpc for purposes of astrometric calculation in this manuscript. The subject of distance is further explored by Barry et al. (2007a).

For the remainder of the paper we report high-resolution N-band observations of the nova RS Ophiuchi using the nulling mode of the 85 meter baseline Keck Interferometer, beginning with a discussion of the nulling mode itself in Section 2. We discuss the observations in Section 3, and the data and analysis in Section 4. In Section 5 we introduce an improved physical model of the system, which unifies all the observations into a coherent framework. The results of this paper and those of other recent observations of RS Oph are discussed in the context of this model in Section 6. Finally, Section 7 contains a summary of our major results and conclusions.

2. The Keck Interferometer Nuller

The Keck Interferometer Nuller (KIN) is designed to address the high-resolution, high-contrast problem of detecting faint emission due, e.g., to an optically-thin dust envelope, at small angular distances from a bright central star. Its operation differs in several ways from the more common fringe scanning optical interferometer. The fundamental measurement quantity is the *null leakage* ,N, which is defined as the ratio of the fringe intensity at the null (i.e., the destructive phase) to the intensity at the peak (the constructive phase). This quantity is measured by switching rapidly between these two phases. It is related to the classical interferometer visibility V by a simple formula:

$$N = \frac{1 - V}{1 + V} \tag{2}$$

Because the instrument operates in the mid-infrared N band centered near 10 μm, the light seen by the detector includes a strong and variable contribution due to thermal emission of the interferometer and telescope optics, and to the terrestrial atmosphere. It is therefore necessary to modulate the coherent astrophysical light at a frequency above the background fluctuations, and to use a lock-in amplifier to detect it. Rather than the traditional approach of wobbling the secondary mirror, the starlight modulation is done interferometrically. This requires a more complicated optical train. Each telescope aperture is split into a pair of equal-sized subapertures. The baselines associated with the split telescope pupils are short ($\sim$ 5 m) compared to the baselines joining the telescopes ($\sim$ 85 m). The Nuller beam combiner sums the fields in these four subapertures after applying an adjustable phase delay to each. The fringe phases are chosen such that the two long baselines share one common phase (π or 0, i.e., destructive or constructive) and the two short baselines share another common phase. One can therefore think of the KIN as having only two baselines, one short and one long.

The short baseline produces fringes spaced at $\frac{\lambda}{D} \sim 400$ mas, which is similar to the size of the primary beam and is assumed to be large compared to the extent of the target object. Modulating its phase therefore modulates the transmitted flux of the entire astronomical source, and the amplitude of this modulated signal is proportional to the flux that passes the fringe produced by the long baseline. The advantage of this approach is the replacement of large tilting secondary mirrors by small flats which need only move a few microns in piston and can therefore operate at high frequency. The moving flats induce no beam-walk and therefore do not modulate the thermal background.

The measurement of the long-baseline fringe phases is interleaved with the measurements of the peak and null intensities. The switching between these various configurations

happens very rapidly, in a cycle that runs at 5 or 2.5 Hz. The long-baseline fringe phases are measured using either of two methods, which are discussed in detail in Serabyn et al., (2007). Briefly, the first method involves sweeping the phase on each long baseline by a wavelength while the other long baseline is shuttered off, and measuring the phase of the resulting sinusoidal intensity variation. The second method involves setting one long baseline to zero (constructive) phase and the other to π (destructive) phase. It can be shown that in this configuration the transmitted flux has a component proportional to the error in the phase of the nulled baseline.

This overall system design permits the visibility to be measured with unusually high precision. The errors in most quantities, including the long-baseline fringe phases and amplitudes, polarization, and wavefront, contribute only second-order and higher terms to the null leakage. Square-law biases are mostly eliminated because the detection of both the peak and null fringes is coherent and linear. Finally, the comparatively long observing wavelength, compared to the more common 2.2 μm or shorter for most other interferometric systems, makes the KIN intrinsically less sensitive to pathlength errors.

While the mathematical foundation for the function of the KIN is thoroughly described in Serabyn et al., (2007) the particular algorithms that we used in the computationally intense modeling of source brightness distributions are given below. These are given for completeness and because these data represent the first scientific result from this instrument.

The positive definite fringe pattern from a monochromatic single-baseline interferometer may be described as

$$F_n(\sigma) = \tfrac{1}{2}(1 \pm \cos(2\pi D_\lambda \cdot \sigma)) \tag{3}$$

in which D_λ is the projected length of the long baseline in units of wavelength and σ is the vector angular distance from the phase center on the celestial sphere. In this expression, the sense of the operator, $\pm$, refers to constructive and destructive combination respectively. Likewise, the cross combiner may be described as

$$F_c(\sigma) = \tfrac{1}{2}(1 \pm \sin(2\pi D'_\lambda \cdot \sigma + \phi)) \tag{4}$$

where D'_λ is the length of the short baseline and the additional term ϕ is an instrument phase delay that allows the fringes to be positioned on the sky.

The monochromatic interferometer response is

$$r_k \equiv \int d\Omega B(\Omega) A(\Omega) F_c(\sigma) F_n(\phi, \sigma) \tag{5}$$

Here, the product $B(\Omega)A(\Omega)$ is a received power differential defined as the product of the source brightness distribution, $B(\Omega)$, and the single-aperture telescope acceptance pattern,

$A(\Omega)$, noting that in these expressions we implicitly assume that both long baselines share the same phase and that both short baselines share the same phase. Choosing the negative sign in each of equations 2 and 3, expanding them using Euler's rule and inserting them into equation 4 results in a sum of nine spatial components. This may be rewritten as

$$r_k(D_\lambda, D'_\lambda, \phi) = \tfrac{1}{2}(N(D_\lambda, 0) \pm Im\{N_d(D_\lambda, D'_\lambda)e^{-i\phi}\} \tag{6}$$

in which the expression $N(D_\lambda, 0)$ is the response that the Keck Nuller would have if it were a simple single-baseline nulling interferometer and the expression, rewritten in terms of the complex visibility, $\hat{V}$, is

$$N_d(D_\lambda, D'_\lambda) \equiv -\tfrac{1}{4}\hat{V}(D'_\lambda + D_\lambda) + \tfrac{1}{2}\hat{V}(D'_\lambda) - \tfrac{1}{4}\hat{V}(D'_\lambda - D_\lambda) \tag{7}$$

is termed the *Keck Nuller response phasor*. A similar expression, $N_c(D_\lambda, D'_\lambda)$, may be derived for the constructive fringe. The interferometric observable or null leakage is given by the dimensionless ratio of these with the destructive *Keck Nuller response phasor* in the numerator.

Before discussing our observations in detail, we briefly discuss the physical implementation of the nulling interferometry principles discussed above. As mentioned above, the long baseline comes from the separation of the two 10-m Keck telescopes, themselves, (D_λ) while the pupils of the two telescopes are split in half creating two approximately-elliptically shaped pupils separated by 5 m, thus providing a short baseline, D'_λ. The pupils of the long baselines are combined in a modified Mach-Zehnder beamsplitter arrangement (Serabyn & Colavita 1999), which is optimized for maximum symmetry between the two input pupils and this provides the"achromatic" null output. However, unlike a conventional beamsplitting interferometer, where there are two output beams for two input beams, in this configuration there are four output beams for the two input beams, i.e., two null outputs and two bright outputs. The modified Mach-Zehnder configuration used here leaves the two other inputs to the beamsplitter system receiving room temperature blackbody radiation. The two null outputs from the two modified Mach-Zehnder interferometers are next combined in a conventional beamsplitter, called the cross-combiner, thus producing 4 output beams (two null and two bright) that are sent to a mid-infrared camera, low-resolution spectrometer system — the KALI camera. It is the intensity of the two null output beams that are actual physical measurement of the Keck Interferometer Nuller system.

3. Observations

We observed the nova about an hour angle of -2.0 on the Keck Interferometer in nulling mode on 2005 Feb 16 with a total of three observations between day 3.831 and 3.846 post-outburst bracketed with observations of two calibrators stars, ρ Boo and χ UMa. We obtained data in N-band light from 8 to 12.5 μm through both ports of the KALI spectrograph with the gating of data for long baseline phase delay and group delay turned on. The Infrared Astronomical Satellite (IRAS) Low Resolution Spectrometer (LRS) spectra for the calibrator stars were flux-scaled according to the broadband IRAS 12 μm fluxes. We observed the calibrators ρ Boo and χ UMa and used them for flux calibration and to remove telluric features. Although these calibrators are quite bright relative to the source their size and point-symmetry are well known. A journal of observations is presented in Table 1.

Our data analysis involves removing biases and coherently demodulating the short-baseline fringe with the long-baseline fringe tuned to alternate between constructive and destructive phases, combining the results of many measurements to improve the sensitivity, and estimating the part of the null leakage signal that is associated with the finite angular size of the central star. Comparison of the results of null measurements on science target and calibrator stars permits the instrumental leakage - the "system null leakage - to be removed and the off-axis light to be measured.

Sources of noise in the measurements made by this instrument have been well described elsewhere (Koresko et al. 2006), however, we think it is important to outline them here for completeness. The null leakage and intensity spectra include contributions from the astrophysical size of the object, phase and amplitude imbalances, wavefront error, beamtrain vibration, pupil polarization rotation, and pupil overlap mismatch. There are also biases, mostly eliminated by use of sky frames, in the calculated fringe quadratures, caused mainly by thermal background modulation due to residual movement of the mirrors used to shutter the combiner inputs for the long baselines. Another source of error is the KALI spectrometer channel bandpass, which is large enough to produce a significant mismatch at some wavelengths between the center wavelength and the short-baseline stroke OPD. This effect, termed warping, distorts the quadratures and is corrected by a mathematical dewarping step accomplished during calibration. There is also the effect of the partial resolution of extended structure on the long baselines which will cause the flux to be undercounted by some amount depending on the spatial extent and distribution of the emitting region. Compared to the error bars this is a rather small effect for most normal stars, and is unlikely to have much influence on the actual spectrum, though, unless the emission lines are coming from a very extended shell approaching 25 mas in angular size. We do not expect this to be the case for nova RS Oph at day 3.8.

Other sources of noise include the difference between the band center wavelength for the interferometer and that of the IRAS LRS calibrator, undercounting of stellar flux resulting from glitches in the short-baseline phase tracking, and the chromaticity of the first maximum of the long-baseline fringe. None of these are significant factors. Firstly, the calibration is based not on broadband photometry but on the IRAS LRS spectrum. Secondly, short-baseline tracking glitches happens nearly as frequently on target observations as on calibrator observations so it should have minimal effect on overall calibrated flux. The effect of chromaticity should likewise be negligible because fringe detection is done on a per-spectral-channel basis. As a result, it is only affected by dispersion within the individual KALI spectral channels, which are about 0.3 μm in width. The last, and clearly the most important contributor to measurement noise would be the sky and instrument drifts between target and calibrator. These observations were exceedingly difficult and so were extended temporarily making this a significant effect, which we assume can contribute as much as 10 percent to the measurement error.

4. Data & Analysis

Figure 1 shows two sets of $8-12.5$ μm spectra of RS Oph on day 3.8 post-outburst. The upper plot shows the outer spatial regime which is the dimensionless null leakage spectrum, i.e., the intensity of light remaining after destructive interference divided by the intensity spectrum, plotted against wavelength in microns. The lower plot is the intensity spectrum, which is light principally from the inner 25 mas centered on the source brightness distribution orthogonal to the Keck Interferometer baseline direction - 38 degrees east of north. The null leakage spectrum may be broadly described as a distribution that drops monotonically with increasing wavelength overlaid with wide, emission-like features. The intensity spectrum, with an average flux density of about 22 Jy over the instrument spectral range, may be similarly described but with a continuum that has a saddle shape with a distinct rise at each end. The underlying shape curves sharply upward for wavelengths shorter than approximately 9.7 μm and longer than 12.1 μm. Overlaid on each of these are traces representing simple models of source brightness distributions fit to the data, described below.

We developed a complete mathematical solution and software suite to model the observatory and source brightness distribution, and to conduct exhaustive grid search and monte carlo confidence interval analysis of solution spaces of these models. Using this suite we thoroughly explored three types of models for the source surface brightness distribution; Gaussian, disk, and shell. Limited (u,v) coverage permitted only rotationally-symmetric models with two parameters - size and flux. We used χ^2 minimization to obtain the best

fit models for both the inner and outer spatial regimes simultaneously. Table 2 displays size measurements and flux values along with their respective one - σ confidence interval values.

The measurements made with the two KALI ports are somewhat independent - the data they produce are combined for purposes of fringe tracking, but not for data reduction. The system null and the final calibrated leakage are computed separately for the two ports. The apparent inconsistency detected between the ports is the result of optical alignment drifts at the time of the measurement. In particular, the last calibrator measurement showed a sudden change in the system null for Port 1, while for all the other calibrator measurements the system nulls were stable. We therefore compared our source brightness distribution models against KALI port 2 data alone. Using Spitzer spectra we identified and removed the emission features centered at 8.66, 11.25, 11.52, and 12.26 μm, and the datum at 12.484 μm. We removed the emission feature data because our intention was to model the continuum. We removed the datum at 12.484 μm because points in the longest wavelength spectral channel for both inner and outer spatial regimes diverged strongly indicating a potential problem with those data.

Figure 2 shows the inner and outer spatial regimes from the KIN data together with *Spitzer* data from day 63 (Evans et al. 2006b) . The absolute flux of these data are unscaled and given with a broken ordinate axis for clarity. The frequency range sampled by the KALI spectrometer, 8 - 12.5 μm, covers many important discrete transitions such as molecular rotation-vibration, atomic fine structure, and electronic transitions of atoms, molecules, and ions. This range also samples several important transitions in solids such as silicates found in dust and polycyclic aromatic hydrocarbons (PAHs) formed by the juxtaposition of benzene rings. Spectral features in the KIN data are clearly not resolved by the instrument and are, in the associated *Spitzer* spectrum, also Doppler broadened and blended. As such we can only get an idea of the composition of the ejecta from the inner and outer spatial regime spectra alone.

In efforts to identify the sources of these emission features we took the high resolution *Spitzer* spectra and, using boxcar averaging, down-binned the data until it and the KIN data had the same equivalent resolution. We then identified spectral lines in the full-resolution *Spitzer* spectrum. These are given in Table 3. This table also shows identification of these spectral lines where they are evident in the KIN spectrum. We assumed that forbidden transitions found in the *Spitzer* spectrum were not represented in the KIN spectra as conditions of density and temperature at day 3.8 post-outburst at the source would not have admitted such species. All spectra were continuum normalized prior to analysis and only minimum $1-\sigma$ detections and better are noted. Line fluxes were determined by Gaussian line fitting and de-blending where needed.

We note that Evans et al. (2006a) found spectra in the I, J, H, and K bands on days 11.81 and 20.75 dominated by hydrogen recombination lines including higher members of the Pfund series. Also present in these early spectra were OII and un-ionized helium and oxygen. In the day-63 *Spitzer* data there are Ne VI and Ne II lines (blended with $Pf\alpha$ and $Hu\alpha$ respectively) just outside of the KIN spectral range from which it may be determined that the evolution of the event has advanced into the coronal phase and the medium has become very tenuous as the meta-stable states giving rise to the forbidden lines are no longer collisionally de-excited. The *Spitzer* spectrum given is replete with hydrogen recombination lines. Emission lines that are represented in the Keck Nuller data are also indicated. The final low-resolution datum at 12.2 μm is strongly influenced by and identified with the *Spitzer* 12.3719 μm HI 7-6 $Hu\alpha$ line blended with HI 11-8 at 12.3833 μm. As indicated in Table 3 at least one neutral hydrogen feature is seen in the inner spatial regime that is not evident in the outer. PAHs, such as Coronene, emit strongly at 8.6 and 11.9 μm. Both of these could be represented in the data, with the later, blended with other emission lines, contributing to the rise at the longwards end. It is, however, unlikely that the environment of the nova at day 3.8 would admit existence such molecules. In agreement with *Spitzer* spectrometry conducted on day 63 (Evans et al. 2006b) in which no thermal emission from dust was detected, we see no evidence of dust in the KIN inner spatial regime spectrum due to the complete absence of the 9.6 μm line typical of silicates. The outer spatial regime, however, does show evidence of Si - an important component of dust.

In addition to the evident line radiation emitted in bound-bound transitions, strong continuum radiation is apparent in both KIN spectra. While the continuum was still clearly visible in J, H, I, K bands on February 24 and detectable on April 9 (Evans et al. 2006a), it is readily apparent that it has substantially subsided by day 63 in Figure 2. When we compare the spectra from RS Oph to those from V1187 Sco (Lynch et al. 2006) we note that the continuum given for V1187 Sco is non-Planckian showing an excess longwards of 9 μm and is strongly red as compared to a F5V Kurucz spectrum. Making a direct comparison of the V1187 Sco and RS Oph continua we find that the slope agrees to within 10%. While both free-bound and free-free transition processes lead to emission of continuum radiation, in the MIR spectral range free-free thermal bremsstrahlung dominates. We attribute the drop in continuum radiation evident in Figure 2 to the transition to line-emission cooling mechanisms. Also, by the time *Spitzer* data were taken, the object had become less dense and so the emission coefficient for thermal bremsstrahlung (proportional to number density of protons and electrons) had dropped considerably. The continuum emission is described in detail by Barry et al. (2007b).

Figure ?? gives the AAVSO V-band photometry for the current epoch of this cataclysmic variable star. In this curve centered at about JD 2453983 is a strong depression

in stellar magnitude. Examination of *Spitzer* spectrum JD 2453988 shows broad, rounded spectral features associated with resonances in aggregates of molecules or dust grains. In classical novae, fluctuations in V-band light have been shown to be closely related to rapid changes in mass loss from the primary and have also been shown to be contemporaneous with reprocessing of the light into infrared wavelengths. Taken together, these are strong evidence for a dust creation event during this time period.

5. Model of the evolution of circumstellar material in the post-outburst phase applicable to the KIN data and other high angular resolution observations

One aspect of the RS Oph binary system that has been neglected in the current literature regarding the recent outburst is the effect of the motion of the two stars through the wind created by mass loss from the red giant star. Garcia (1986) suggested that there could be a possible ring of material of diameter less than 40 AU around the RS Oph binary system or possibly surrounding the red giant component, based on his measurements of an absorption feature in the core of the Fe II emission line profile at 5197 angstroms. The observations were performed in 1982 and 1983, several years before the 1986 nova outburst.

Subsequently, and motivated by somewhat different observations, Mastrodemos and Morris (1999) computed three-dimensional hydrodynamical models of the detached white dwarf companion on the dusty winds from red giant and asymptotic giant branch stars. Their purpose was to see if these models could reproduce some of the observed characteristics of axisymmetric or bipolar pre-planetary nebulae. Their study focused on a parameter space that encompassed outflow velocities from 10 to 26 km/s, circular orbits with binary separations from 3.6 to 50 AU, and binary companions having a mass range of 0.25 to 2 $M_{\odot}$. For binary separations of about 3.6 AU and mass ratios of 1.5, it was possible to generate a single spiral shock that winds 2-3 times around the binary before it dissipates at > 25 times the radius of the RG star. There is an density enhancement of about a factor of 100 over the normal density in the wind in the plane of the orbit of the two stars, and an under density or evacuated region perpendicular to the plane of the orbit. Observational support for this model was found recently by Mauron & Huggins (2006) who observed a spiral pattern around the AGB star AFGL 3068 that was consistent with the model of Mastrodemos and Morris. The underlying binary, a red giant and white dwarf, was discovered by Morris et al. (2006), who also determined the binary separation and hence approximate orbital period, which was consistent with expectations from the appearance of the spiral nebula pattern seen by Mauron & Huggins and the model.

Figure 5 shows the geometry of the nebula in the plane of the orbit of the RS Oph

system based on the generally adopted parameters for the system, including an orbital period of 460 days, and an inclination angle of about 33 degrees, for the epoch just prior to the nova outburst. The spiral shock model produces an archmedian spiral nebula, with the separation between adjacent windings of about 3.3 mas based on the period noted above and a wind speed from the red giant star of 20 km/s. Note that we expect there should be about 17 such rings created between outbursts, with the overall size of the nebula of the order of 100 mas.

In order to better understand the Keck Nuller observations and other high angular resolution observations, we have modeled the evolution of the circumstellar nebula following the outburst, which we display in Figures 6-9. For the purposes of this discussion, we adopt the model of Hachisu and Kato (2001), but with the simplifcation of a flat accretion disk geometry, i.e., not warped as in their paper. We leave the details of our calculations to another paper (Danchi & Barry 2007).

The results are of fundamental importance to the interpretation of the data, and we begin with the most immediate effect after the blast, which is the sublimation of dust within a zone where the temperature of a blackbody dust grain would be > 1500 K in equilibrium. Figure 6 displays the evolution of the dust sublimation radius, which is roughly 4-5 mas until about day 70, after which it steadily declines to $<<$ 1 mas about 250 days after the outburst. This means that much or all of the dust within this zone has entered the gaseous phase, except for a small "sliver" of material in the shadow of the red giant star. This provides a reservoir of hot gas that is subsequently affected by the blast wave passing through within the next few days.

As the two stars move relative to each other in their orbit about their common center of mass, the location of the shadow of the nova moves, and consequently the material in the shadow that has not been affected by the blast wave from the nova will be sublimated during this luminous phase, creating hot gas in the vicinity within a few mas of the stars. This material may still have the type of repeating density structure that was initially present, and may be observable with high angular resolution instrumentation.

Another effect, also which is essentially immediate, is the heating of the surface of the red giant star that faces the nova, as seen in Figure 7. Our calculations indicate that this side of the red giant star increases from about 3400 K to as much as 4200 K within a few days past the outburst. The temperature steadily declines from day 70 until it reaches equilibrium with the other side around day 250. This rapidly heated gas from the photosphere of the red giant star can also provide a reservoir of material that will be affected during the period of time past when the blast wave hits, which is less than one day from the eruption.

Figure 8 displays a schematic view of the system geometry from days 4 to 90 after the recent outburst. Assuming typical wind velocities of about 20 km/s for the red giant wind, there are roughly 17 rings separated by approximately 3.3 mas that form between RS Oph outbursts. The top left panel displays the system geometry at 4 days post-outburst. A gray ring is drawn in the center of the figure to indicate the size of the region affected by the blast at this epoch. In (a) the outer part of the spiral is overlayed with light gray to indicate that it is not known if the material stays in a coherent spiral past the first few turns. The diameter of the shocked region is about 5 mas assuming the blast wave travels at a velocity of 1730 km/s in the plane of the orbit. In (b) the top right panel the blast wave is now about 13 mas in diameter on day 21. By day 57 the blast wave is about 36 mas in diameter as shown the bottom left panel, Fig. 8(c). At day 90 the blast wave has traversed the entire spiral pattern. The density at the outer edge of the original spiral could be as much as 1000 times the density that would exist otherwise in a uniform outflow from the red giant star, depending on how efficiently the blast wave transports material from the inner part of the spiral pattern outwards. We show the extreme case in which the blast wave is 100% efficient in creating a ring-like structure that propagates outward from the system.

The evolution of the luminosity of the red giant and nova is also significant in aiding our understanding of the observations. Figure 9 (a) displays computed V band light curves up to day 250 after the outburst including the effect of the irradiation of the accretion disk and the irradiation of the red giant star by the nova. Note this calculation overestimates the total luminosity of the nova compared to the V band light curve displayed in Figure 4 during the period from about 10 days to about 50 days, and this is likely due to the simplified disk geometry that we have employed in our own calculations. Most importantly these light curves show that the V band luminosity is dominated by the nova for about the first 50-70 days, and after that the red giant star dominates the V band luminosity. This is significant as most telescopes track on V band light (including interferometers) and the tracking center then moves by a mas or so during the post-outburst evolution of the system. H band luminosity evolution is plotted in Fig. 7(b), and is different than that of the V band evolution. At H band the nova dominates the luminosity only for the first 5 days or so, and after that the H band light curve is completely dominated by the red giant star. This means the phase center for fringe detection is offset from that of the tracking center from days 5 onward by a mas or so, as mentioned above. The N band luminosity, displayed in Fig. 9(c), evolves like that of the H band, and the nova dominates the mid-infrared light only up to day 4. After that there is an offset between the tracking center and N band fringe center like that noted for the H band.

6. Implications to the interpretation of the Keck Nuller and other high-angular resolution observations

We now reexamine data from the 2006 outburst within the framework of the spiral shock model of the geometry of RS Oph presented in the last section. In its simplest form, this geometry evolves into a geometry favorable to create a bipolar geometry for the radio emission from the outburst that was discussed by O'Brien et al. (2006), as seen in Figure 8(d).

Such a geometry provides a natural explanation for some of the differences between the measurements, as the blast wave would be restricted and slowed in the orbital plane due to the high density regions, while its flow would be relatively unimpeded perpendicular to that plane. This corresponds well to what was observed by Chesneau et al. (2006), where the observed velocity components came from distinctly different position angles. These authors also calculate that the red giant star should be a a position angle of about 150-170 degrees at the time of the outburst. The inclination angle is not particular well established but is expected to be approximately 30-40 degrees relative to the line of sight. Thus the plane of the orbit is such that the high velocity flow would be expected to be mostly East-West and the the continuum emission would have an elliptical shape with the position angle measured by Chesneau et al. (2006). Furthermore, the spiral shock wave tends to have the largest densities near the white dwarf star and on the opposite side of the red giant star, the separation being of the order of two to four times the separation between the two stars, i.e., a few mas. The larger separation occurs when the red giant star has been spun up so that it synchronous with the orbital motion. Thus it is possible that some of the data can be interpreted in terms of emission from hot clumps of material within the spiral shocks. Detailed radiative transfer calculations will need to be performed to refine this model.

There is a wealth of recent observational work on RS Oph across the spectrum from X-ray (Sokoloski), near-infrared (Evans et al. 2006, Chesneau et al. 2007, Das et al. 2006), radio (O'Brien et al. 2006), and now mid-infrared (this work). Generally speaking, the observational picture is consistent with the thermonuclear runaway model as described by Bode & Kahn (1985). Extensive modeling of the light curves has been performed by Hachisu & Kato (2000, 2001), which include effects such as the irradiation of the red giant star by the white dwarf, and the accretion disk, which become important about 4 days post-outburst, and which are the basis for our own calculations presented in Figs. 6,7, and 9. In this general picture the recurrent nova differs from a classical nova in that the high-velocity ejecta from the WD is impeded by the wind from the red giant star, which in turn generates a shock wave that propagates through the red giant wind. Observations of the shock wave in the near-infrared by Das et al. (2006) confirm this picture and trace the evolution of the widths

of Pa β and O I lines as a function of time post-outburst, and clearly show the expected free-expansion phase of the shock ended about 4 days post-outburst.

Most of the observational work has used spectroscopic methods, and only the interferometric observations are capable of spatially separating the various components of RS Oph that contribute to the emission that is seen spectroscopically. Chesneau et al. (2007) observed RS Oph 5.5 days post-outburst in the continuum at 2.13 μm, Br γ at 2.17 μm, and He I at 2.06 μm with the AMBER instrument on the VLTI. They fitted their data with uniform ellipses, gaussian ellipses, and a uniform ring. The models had excellent consistency in terms of the position angle of the ellipse (140 degrees) and the ratio between minor and major axes (0.6). For the continuum at 2.13 μm, a uniform ellipse had a major axis of 4.9 $\pm$ 0.4 and minor axis 3.0 $\pm$ 0.3 mas, while the gaussian ellipse had a major axis of 3.1 $\pm$ 0.2 and minor axis of 1.9 $\pm$ 0.3 (FWHM). These measurements are consistent with the expected size of the shocked region at the epoch of their measurements.

Monnier et al. (2006) presented IOTA results in the near-infrared bands at H and K, and had somewhat different conclusions than some of the other workers because they were able to fit their visibility and closure phase data best with a binary model with two sources separated by 3.13 $\pm$ 0.12 mas, position angle of 36 $\pm$ 10 degrees, and brightness ratio of 0.42 $\pm$ 0.06. Their gaussian fits at 2.2 μm gave a FWHM of 2.56 $\pm$ 0.24 mas for the same period of time as the AMBER observations. A striking feature of those results is that size of the emitting region decreased 10-20 % between about days 4 and 65 post-outburst. For example, the size at 2.2 μm actually decreased from about 2.6 to 2.0 mas (FWHM), while at 1.65 μm, the size decreased from 3.3 to 2.9 mas. However the 2 μm continuum sizes are in approximate agreement. Monnier et al. (2006) rule out an expanding fireball model, however, they would have over-resolved the fireball anyway since it would be at least 8 mas in diameter, for a distance of 1600 pc, or a substantially larger angular size if the distance were smaller. This interpretation remains problematic.

However, their results are consistent with an emitting region at 10 μm that is somewhat larger than that seen at 2 μm, for example, our data are fitted by a gaussian 4.0 $\pm$ 0.4 mas (FWHM), while the IOTA data had a size of 2.6 $\pm$ 0.2 mas. By 4 days post-outburst, a spherical shock wave would be expected to have a radius of about 4 mas assuming a speed of approximately 1400 km/s and a distance of 1.6 kpc. Thus, according to this simple model, all the interferometric IR continuum emission should be coming from within the post-shock region. The AMBER/VLTI results indicate a more complex picture of the velocity field of the expanding material, with two indicated - a "slow" field between -1800 and 1800 km/s, and a "fast" one between -3000/-1800 km/s and 1800/3000 km/s. The position angle of the emitting material for the two velocity groups differ, with the "fast" component being well

defined in the East-West (position angle 90 or 270 degrees ± 5 degrees) direction and the "slow" component with position angles from 55 to 110 degrees modulo 180 degrees.

The spiral shock model is clearly relevant to the interpretation of the IOTA data presented in Monnier et al. (2006). As noted above, the increased density of gas and dust in the arms of the spiral would certainly provide an impediment to the free expansion of the fireball, as well as provide a reservoir of hot material that would emit strongly at 2 μm. Their data indicate a closure phase that is consistent with zero or 180 degrees for the first epoch (days 4-11) and convincingly non-zero only for hour angles from -1.5 to -1 hr on the second epoch (days 14-29), and at +1/2 hr on the third epoch (days 49-65). Hence, the closure phase signals and the binary interpretation may be more consistent with hot clumpy material that is cooling off and will condense into dust as the white dwarf star cools off from its most luminous state, i.e., as shown in Fig. 6. Note that the sublimation radius rapidly decreases from $\sim$ 5 mas to about 2 mas from day 70 to day 120. Furthermore, as the luminosity changes, the star tracker on IOTA may be providing at different optical center to the fringe detection system, since in the first few days during the outburst the optical emission is dominated by the white dwarf star itself, whereas after it has cooled, the optical emission is dominated by the red giant star. Thus the effects change in the optical tracking and interferometric phase center will need to be included in the analysis to properly interpret the data. The offset between the optical tracking center and the fringe phase center can cause a miscalibration of the visibility. Since the 2 μm emitting region is actually decreasing in size with time, as seen in their Fig. 1 and Table 2, it seems more likely they are observing the cooling of this hot material near the two stars than actually resolving the binary, however, the effects of the material in the shadow of the red giant star must be included in the interpretation of the near-infrared and mid-infrared data.

7. Summary and Conclusions

We have analyzed data from the recurrent nova RS Oph for the epoch around 4 days post-outburst using the new Keck Interferometer Nuller (KIN) instrument. These data allowed us to determine the size of the emitting region around the RS Oph at wavelengths from 8-12 μm. By fitting the unique KIN inner and outer spatial regime data, we have obtained an angular size of the mid-infrared continuum of 6.2, 4.0, or 5.4 mas for a disk profile, gaussian profile (fwhm), and shell profile respectively. The data show evidence of enhanced neutral atomic hydrogen emission located in the inner spatial regime relative to the outer regime. There is also evidence of a 9.7 μm silicate feature seen outside of this region, which is consistent with dust that had condensed prior to the outburst, and which has not yet

been disturbed by the blast wave from the nova. Our analysis of the observations, including the new ones presented in this paper, are most consistent with a new physical model of RS Oph, in which spiral shock waves associated with the motion of the two stars through the cool wind from the red giant create density enhancements within the plane of their orbital motion. This model has sufficient complexity to explain the apparent disagreements between the various measurements. Indeed all the measurements are consistent with this type of model. Clearly further observations are warranted to more fully characterize this interesting and complex system.

We are grateful to the National Aeronautics and Space Administration, Jet Propulsion Laboratory, the California Association for Research in Astronomy, the Harvard-Smithsonian Center for Astrophysics, and to the National Aeronautics and Space Administration, Goddard Space Flight Center for support of this research. We acknowledge with thanks the variable star observations from the AAVSO International Database contributed by observers worldwide and used in this research. The data presented herein were obtained at the W.M. Keck Observatory, which is operated as a scientific partnership among the California Institute of Technology, the University of California and the National Aeronautics and Space Administration. The Observatory was made possible by the generous financial support of the W.M. Keck Foundation. One of the authors (RKB) would also like to acknowledge Eugene E. Rudd of the United States Naval Research Laboratory for his continued support and encouragement.

Facilities: Spitzer, IOTA, Keck:I, Keck:II.

REFERENCES

Adams, W. S., Joy, A. H., 1933, PASP, 45, 249a

Barbon, R., Mammano, A., Rosino, L., 1969, Comm. Konkoly Obs., 65, 257

Barry, R.K., Sokoloski, J. , Hachisu, I., Evans, A., Mikolajewska, J., Rupin, M., Mukai, K., Gehrz, R., 2007, Proc. RS Oph 2006 Epoch, Keele University, Keele UK, manuscript in preparation

Barry, R. K., Skopal, A., Danchi, W. C., 2007, ApJ, manuscript in preparation

Blair, W. P., Stencel, R. E., Feibelman, W. A., Michalitsianos, A. G., 1983, ApJS, 53, 573B

Bode, M. F., Kahn, F. D., 1985, MNRAS, 217, 205

Cardelli, J. A., Clayton, G. C., Mathis, J. S., 1989, ApJ, 345, 245

Cassatella, A., Harris, A. Snijders, M. A. J., Hassall, B. J. M., 1985, Proc. ESA Workshop: Recent Results on Cataclysmic Variables, ESA SP-236

Chesneau, O., Nardetto, N., Millour, F., Hummel, C., Domiciano de Souza, A., Bonneau, D., Vannier, M., Rantakyro, F., Spang, A., Malbet, F., Mourard, D., Bode, M. F., OBrien, T. J., Skinner, G., Petrov, R. G., Stee, P., Tatulli, E., Vakili, F., 2007, A&A

Creech-Eakman, M.J., Moore, J.D., Palmer, D.L., Serabyn, E., 2003, Proc. SPIE, 4841, 330c

Danchi, W.C., & Barry, R., 2007, manuscript in preparation

Das, R., Banerjee, D.P.K., & Ashok, N.M. 2006, ApJ, 653, 141

Dobrzycka, D., Kenyon, S. J., 1994, ApJ, 108, 2259

Downes, R. A., Duerbeck, H. W., 2000, ApJ, 120, 2007

Evans, A., Kerr, T., Yang, B., Matsuoka, Y., Tsuzuki, Y., Bode, M. F., Eyres, S. P. S., Geballe, T. R., Woodward, C. E., Gehrz, R. D., Lynch, D. K., Rudy, R. J., Russell, R. W., O'Brien, T. J., Starrfield, S. G., Davis, R. J., Ness, J.-U., Drake, J., Osborne, J. P., Page, K. L., Adamson, A., Schwarz, G., Krautter, J. 2006, MNRAS, 374, 1

Evans, A., Woodward, C.E., Helton, A., Gehrz, R. D., Lynch, D. K., Rudy, R. J., Russell, R. W., Bode, M. F., Kerr, T., Yang, B., Matsuoka, Y., Tsuzuki, Y., Eyres, S. P. S., Geballe, T. R., O'Brien, T. J., Davis, R. J., Starrfield,S. G., Ness, J.-U., Drake, J., Osborne, J. P., Page, K. L., Schwarz, G., Krautter,J., 2006, ApJ, manuscript in preparation

Fekel, F. C., Joyce, R. R., Hinkle, K. H., Skrutskie, M. F., 2000, ApJ, 119, 1375

Garcia, M.R., 1986, AJ, 91,1400

Fleming, W., 1904, Harvard College Observatory Circular, 76

Hachisu, I., Kato, M., 2000, ApJ, 536, 93

Hachisu, I., Kato, M., 2001, ApJ, 558, 323

Hjellming, R. M., van Gorkom, J. H., Taylor, A. R., Seaquist, E. R., Padin, S., Davis, R. J., Bode, M. F., 1986, ApJ, 305, 71

Kenyon, S. J., Fernandez-Castro, T., 1987, ApJ, 93, 938

Kenyon, S. J., Gallagher, J. S., 1983, AJ, 88, 666K

Koresko, C., Colavita, M., Serabyn, E., Booth, A., Garcia, J., 2006, Proc. SPIE, 6268, 626816-1

Lynch, D. K.; Woodward, C. E.; Geballe, T. R.; Russell, R. W.; Rudy, R. J.; Venturini, C. C.; Schwarz, G. J.; Gehrz, R. D.; Smith, N.; Lyke, J. E.; Bus, S. J.; Sitko, M. L.; Harrison, T. E.; Fisher, S.; Eyres, S. P.; Evans, A.; Shore, S. N.; Starrfield, S.; Bode, M. F.; Greenhouse, M. A.; Hauschildt, P. H.; Truran, J. W.; Williams, R. E.; Perry, R. Brad; Zamanov, R.; O'Brien, T. J., 2006, ApJ, 638, 987

Mastrodemos, N., & Morris, M., 1999, ApJ, 523, 357

Mauron, N., & Huggins, P.J., 2006, A&A, 452, 257

Monnier, J.D., Barry, R.K., Traub, W.A., Lane, B.F., Akeson, R.L., Ragland, S., Schuller, P.A., Berger, J.P., Millan-Gabet, R., Pedretti, E., Schloerb, F.P., Koresko, C., Carleton, N.P., Lacasse, M.G., Kern, P., Malbet, F., Perraut, K., Muterspaugh, M.W., 2006, ApJ, 647, 127

Morris, M., Sahai, R., Matthews, K., Cheng, J., Lu, J., Claussen, M., Sanchez-Contreras, C., 2006, in Planetary Nebulae in our Galaxy and Beyond, Proceedings of IAU Symposium No. 234, M. J. Barlow & R. H. Mendez, eds., 469.

Morrison, W., 1985, IAU Circ., 4030

Mürset, U., & Schmid, H.M., 1999, A&AS, 137, 473

Narumi, H., Hirosawa, K., Kanai, K., Renz, W., Pereira, A.,Nakano, S., Nakamura, Y., & Pojmanski, G. 2006, IAU Circ., 8671, 2

O'Brien, T. J., Bode, M. F., Porcas, R. W., Muxlow, W. B., Eyres, S. P. S., Beswick, R. J., Garrington, S. T., Davis, R. J., Evans, A., 2006, Nature, 442, 279

Oppenheimer, B.D., Mattei, J.A., 1993, JAVSO, 22, 1050

Payne-Gaposchkin, C., 1957, The Galactic Novae, North-Holland, Amsterdam

Payne-Gaposchkin, C., 1977, AJ, 82, 665

Pottasch, S. R., 1967, Bull. Astron. Inst. Netherlands, 19, 227

Rupin, M. P., Mioduszweski, A. J., Sokoloski, J. L., Kaiser, C. R., Brocksopp, C., 2006, Proc. AAS

Schaeffer B., 2004, IAUC 8396

Serabyn, E., Kuchner, M., Menneson, B., Traub, W., et al., 2007, ApJ, manuscript in preparation

Snijders, M. A. J., 1985, Ap&SS, 130, 244

Sokoloski, J.L., Luna, G.J.M., Mukai, K., Kenyon, S.J., 2006, Nature, 442, 276

Walerstein, G., 1958, PASP, 70, 537w

Table 1. Observing Log for RS Ophiuchi.

Object	Type	Time (UT)	U (m)	V (m)	Airmass
Chi UMa	cal	15:07:07	23.85	80.61	1.38
Chi UMa	cal	15:15:39	21.92	81.25	1.41
RS Oph	trg	15:50:15	54.57	64.75	1.46
RS Oph	trg	16:03:46	55.35	64.37	1.39
RS Oph	trg	16:12:35	55.75	64.12	1.35
Rho Boo	cal	16:34:24	39.63	75.14	1.08

Table 2. RS Ophiuchi model fitting results.

Source Model	Angular Size (mas) (N band)	Radiant Flux (Jy)	Major Size (mas) (K band)	Minor size[a] (mas) (K band)
Uniform Disk	$6.2^{+0.2}_{-0.5}$	$22.4^{+3.9}_{-3.7}$	4.9 ± 0.4	3.0 ± 0.3
Uniform Gaussian[b]	$4.0^{+0.4}_{-0.4}$	$22.4^{+3.8}_{-3.7}$	3.1 ± 0.2	1.9 ± 0.3
Uniform Shell[c]	$5.4^{+0.5}_{-0.5}$	$22.4^{+3.8}_{-3.7}$	3.7 ± 0.3	1.9 ± 0.2

[a]Sizes for continuum values at 2.3 μm after Chesneau et al. (2007).

[b]Full width at half maximum.

[c]Spherical shell with thickness 1.0 mas - optically thin.

Table 3. Mid Infrared Line List.

Wavelength (μm)	ID	*Spitzer* 4/16 (Jy)	*Spitzer* 4/26 (Jy)	KIN (Inner)	KIN (Outer)
7.46	$Pf\alpha - HI: 6-5$ [a]	detected	detected	[b]	
7.6524	$[NeVI]$	detected	detected		
8.76	$HI: 10-7$	0.04	0.04	0.05	0.05
8.991	$[ArIII]$	0.02	0.02	0.02	0.02
9.407	SiI	0.02	0.02	0.03	0.03
9.7178	NeI	0.02	0.02	0.03	0.03
10.5035	$HI: 12-8$	0.03	0.03	0.03	0.03
11.3087	$HI: 9-7$	0.05	0.06	0.06	0.06
11.539	$HI: 15-9$	0.02	0.01	0.01	
12.3719	$Hu\alpha$	0.16	0.17	0.17	0.17
12.8135	$[NeII]$	0.02	0.02	0.01	0.01

[a]Estimated.

[b]Influences particular KIN spatial regime.

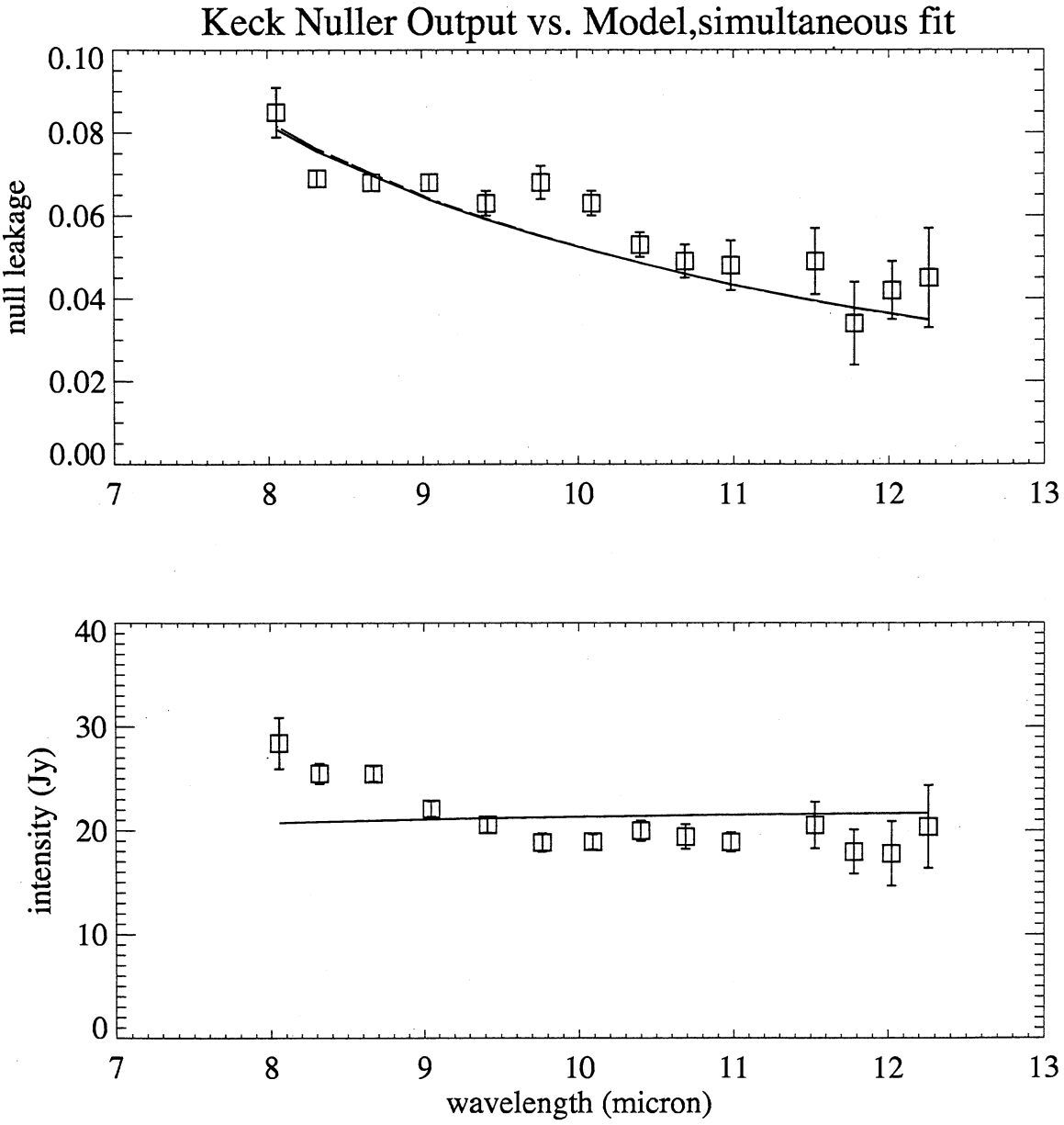

Fig. 1.— Plot of three best-fit continuum models against Keck Nuller data. All three models; disk, shell, and Gaussian, that minimized χ^2 simultaneously against the null leakage and intensity spectra, lie effectively on top of one another. The top trace gives the dimensionless null leakage or interferometric observable which is the null fringe output divided by the intensity spectrum. The lower trace is the constructive fringe output or intensity spectrum. As indicated in the text we have removed five data points from the original set - four emission features and one bad datum - for the purpose of fitting the continuum.

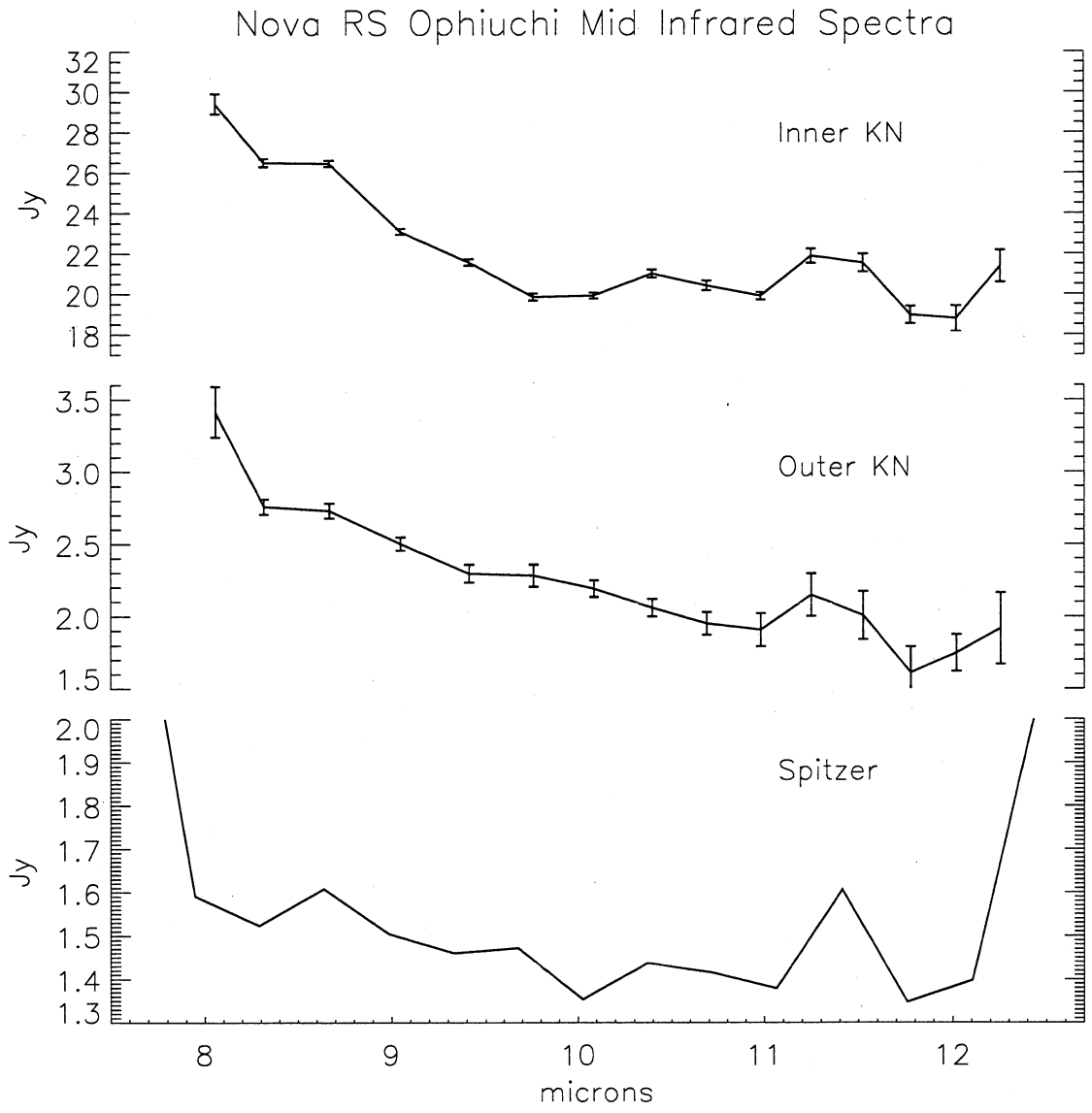

Fig. 2.— Plot of Keck Interferemeter Nuller spectra together with a *Spitzer* spectrum. Upper trace is the intensity spectrum or inner KIN spatial regime - light dominated by the inner 25 mas about the center of the source brightness distribution at mid band. The middle trace is the nulled fringe output which is the interferometric observable times the intensity spectrum. This is the outer spatial regime - light emitted by material greater than about 12 mas from the center of the source. The lower trace is *Spitzer* data from day 63 boxcar averaged to yield approximately the same spectral resolution as the Keck Interferometer Nuller. None of the data were continuum normalized. Note especially the features between 9 and 11 microns and how the inner and outer spatial regime spectra are different from one another.

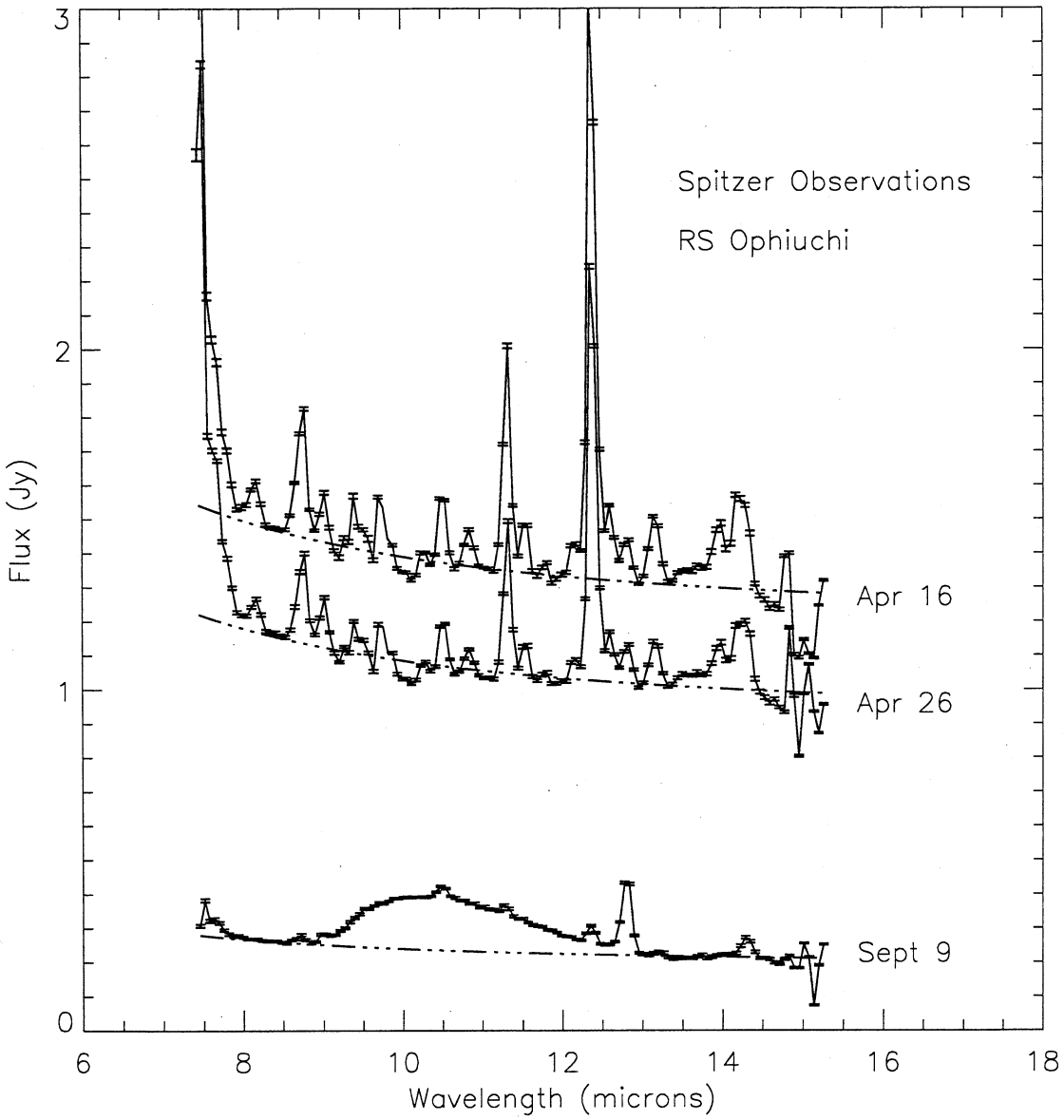

Fig. 3.— Continuum measurements of data from 4/16, 4/26, 9/9 and 10/10/06. Here we see that the continuum drops rapidly as time advances with the spectral emission features almost identical on days 4/16 and 4/26. Data obtained on 9/9 is starkly different with a strong solid-state feature evident between 9 and 13 microns.

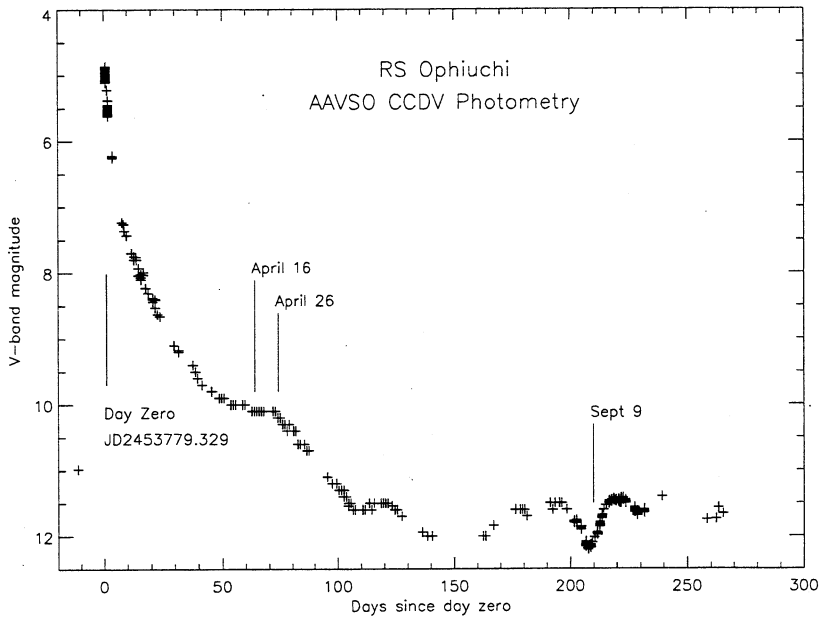

Fig. 4.— AAVSO photometry with $T_2 = 4.75$ days and $T_3 = 10.19$ days indicated. Note the end of the plateau phase on 4/16/06 - evidence of hydrogen burning turnoff. Note the evident strong fluctuation of V-band brightness about 9/9/06. This is strong evidence of a dust creation event.

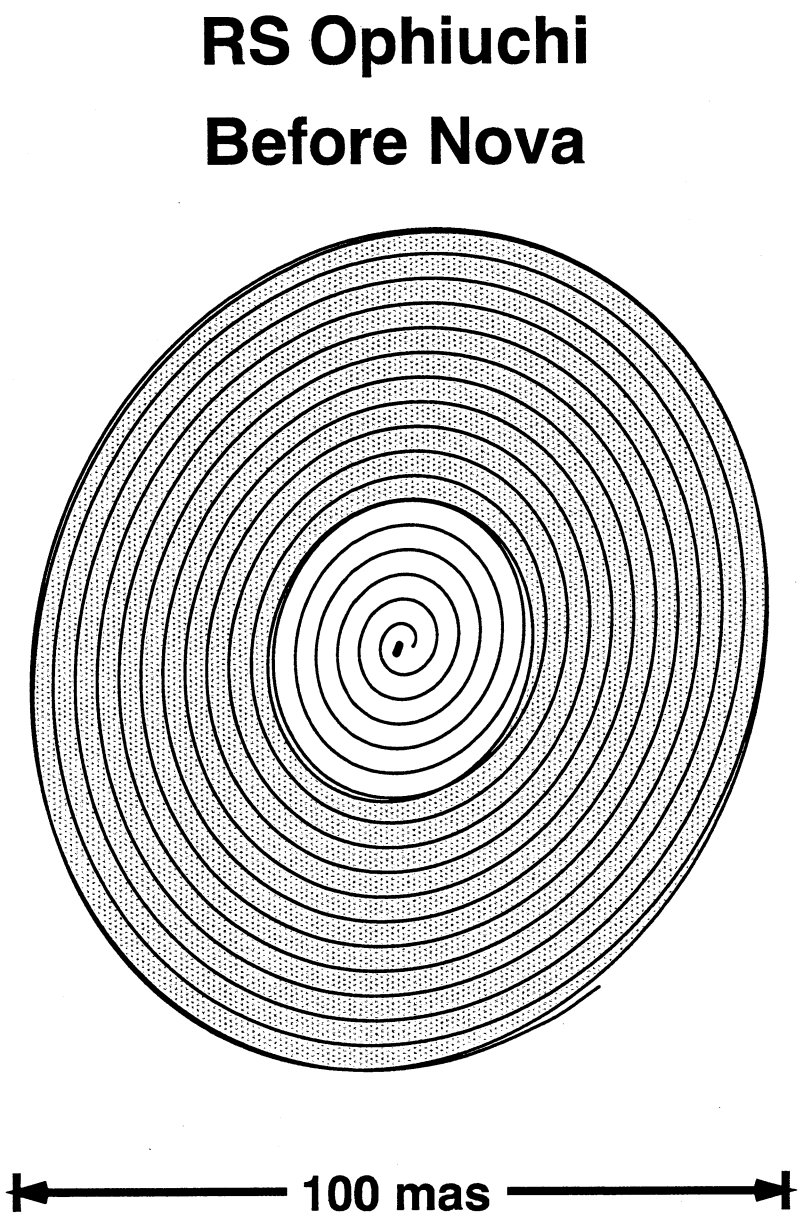

Fig. 5.— Theoretical diagram of circumstellar material surrounding the binary RS Oph before the nova eruption. The interaction of the white dwarf and red giant star in the slow dense wind of the red giant star can create a spiral shock with an enhanced density in the plane of the orbit of the two stars. The overall size of the dense in-plane material is of the order of 100 mas if RS Oph is at a distance of 1600 pc and the wind speed is about 20 km/s.

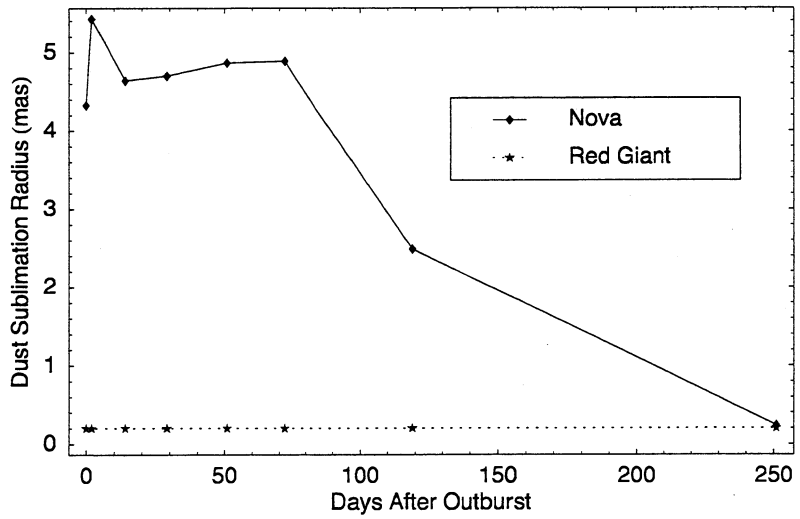

Fig. 6.— Sublimation radius of dust (mas) as a function of the number of days post-outburst for the Nova and for the red giant companion.

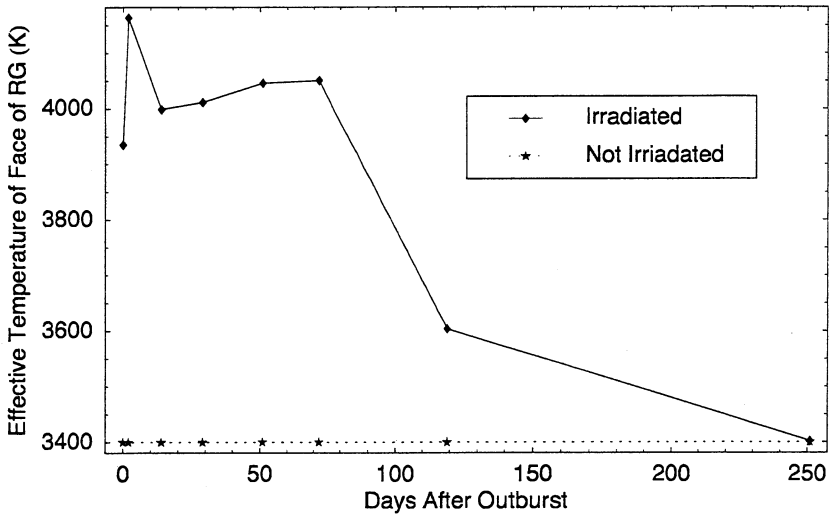

Fig. 7.— Temperature of red giant star for the surface that is facing the Nova as a function of the number of days post-outburst. Also plotted is the temperature of the non-irradiated side of the red giant.

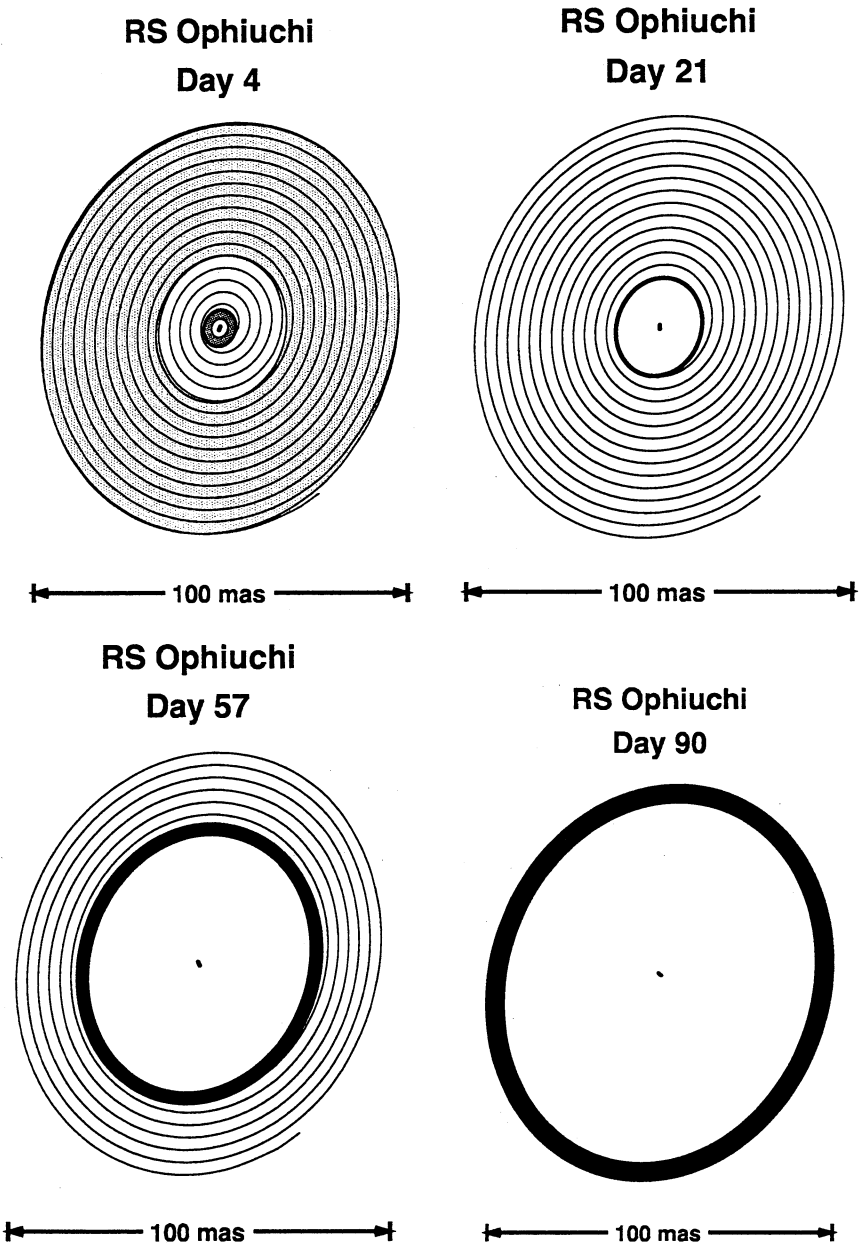

Fig. 8.— Spiral shock wave model of RS Oph. (a) Top left panel displays the system geometry at 4 days post-outburst. A gray ring is drawn in the center of the figure to indicate the size of the shocked region at this epoch. The outer part of the spiral is overlayed with light gray to indicate that it is not known if the material stays in a coherent spiral past the first several turns. The diameter of the shocked region is about 5 mas assuming the blast wave travels at a velocity of 1730 km/s in the plane of the orbit. (b) Top right panel. The blast wave is now about 13 mas in diameter on day 21. (c) Bottom left panel. The blast wave is about 36 mas in diameter on day 57. (d) Bottom right panel. By day 90 the blast wave has traversed the entire spiral pattern. The density at the outer edge of the original spiral could be as much as 1000 times the density that would exist otherwise in a uniform outflow from the red giant star.

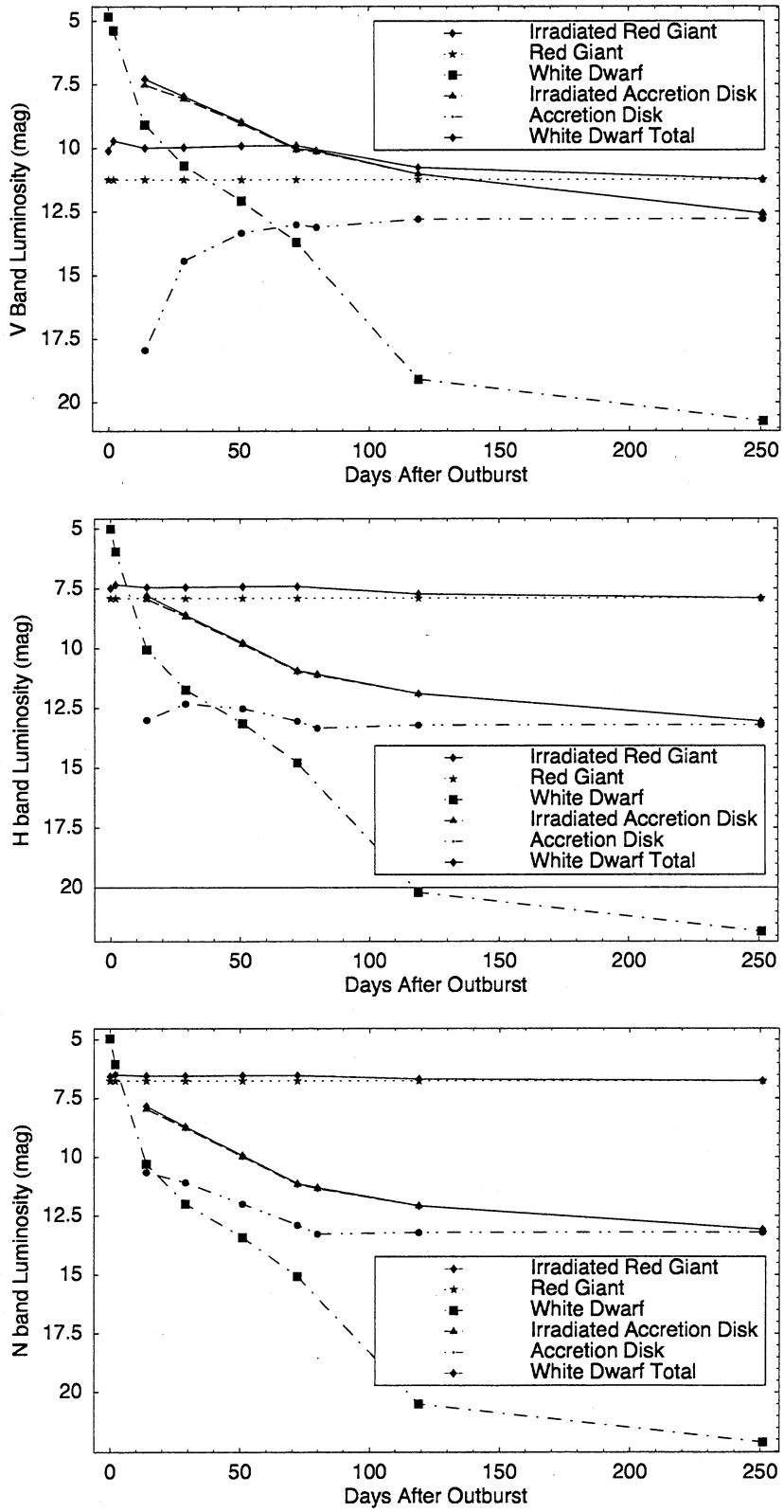

Fig. 9.— (a) V Band luminosity as a function of time for Nova and red giant components of binary system.(b) H band luminosity evolution. (c) N band luminosity evolution.